Draft version September 24, 2014
Preprint typeset using LaTeX style emulateapj v. 05/12/14

STRIPPED ELLIPTICAL GALAXIES AS PROBES OF ICM PHYSICS: I. TAILS, WAKES, AND FLOW PATTERNS IN AND AROUND STRIPPED ELLIPTICALS

E. Roediger[1,5], R. P. Kraft[2], P. E. J. Nulsen[2], W. R. Forman[2], M. Machacek[2], S. Randall[2], C. Jones[2], E. Churazov[3], R. Kokotanekova[4]

[1]Hamburger Sternwarte, Universität Hamburg, Gojensbergsweg 112, D-21029 Hamburg, Germany
[2]Harvard/Smithsonian Center for Astrophysics, 60 Garden Street MS-4, Cambridge, MA 02138, USA
[3]MPI für Astrophysik, Karl-Schwarzschild-Str. 1, Garching 85741, Germany
[4]AstroMundus Master Programme, University of Innsbruck, Technikerstr. 25/8, 6020 Innsbruck, Austria

Draft version September 24, 2014

ABSTRACT

Elliptical cluster galaxies are successively stripped of their gaseous atmospheres due to their motion through the intra-cluster medium (ICM). The stripped galactic gas forms a 'tail' in the galaxy's wake. Deep X-ray observations reveal the fine-structure of the gas tail and of the interface between galactic gas and ICM. This fine-structure depends on dynamic conditions (galaxy potential, initial gas contents, orbit in the host cluster), stripping stage (early infall, pre-/post-pericenter passage), as well as on the still ill-constrained ICM plasma properties (thermal conductivity, viscosity, magnetic field structure). In a series of papers, we aim at disentangling dynamic and plasma effects in order to use observed stripped ellipticals as probes of the ICM plasma properties. This first paper investigates the detailed dynamics of successive gas stripping by means of inviscid hydrodynamical simulations. We distinguish a long-lasting initial relaxation phase and a quasi-steady stripping phase. During quasi-steady stripping, the flow of ICM *around* the remnant atmosphere is similar to the well-known flow around solid bodies. The galaxy's near wake is characterized by a 'deadwater' region that extends ~ 1.5 galactic atmosphere lengths into the downstream direction. Only in the far wake, i.e., beyond the deadwater region, can stripped galactic gas be carried away from the galaxy. Simultaneously, the size and shape of the galaxy's remnant atmosphere is shaped by the ambient flow in three distinct regions: (i) The upstream atmosphere is pushed back such that pressure balance between the atmosphere and the ambient ICM is maintained. (ii) Gas removal takes place predominantly at the sides of the remnant atmosphere via Kelvin-Helmholtz instabilities. (iii) The downstream atmosphere is shaped into a tail because it is shielded from the ICM wind and thus is not stripped easily. Observationally, both, this 'remnant tail' as well as the stripped gas in the wake can appear as a 'tail', but only stripped galactic gas in the wake mixes with the ambient ICM. The remnant tail contains only unstripped, unmixed galactic gas. Paper II of this series describes the effect of viscosity on flow patterns and resulting observable features. While the qualitative results are generic, we aim at the most direct comparison to observations and tailored our simulations to the Virgo elliptical galaxy M89 (NGC 4552). Paper III of this series compares in detail new deep Chandra and archival XMM-Newton observations to our simulations.

Keywords: clusters: individual: Virgo – galaxies: M89 – simulations

1. INTRODUCTION

Elliptical galaxies falling into clusters are successively stripped of their gaseous atmospheres due to their motion through the intra-cluster medium (ICM) (Nulsen 1982; Gisler, G. R. 1976; Takeda et al. 1984; Stevens et al. 1999; Toniazzo & Schindler 2001; Acreman et al. 2003; McCarthy et al. 2008, among others). Stripped ellipticals display four basic features: A galactic atmosphere truncated in size, a downstream tail of galactic gas, an upstream contact discontinuity between the galactic atmosphere and the hotter ICM, and generally a bow shock ahead of the galaxy due to their typically supersonic motion. The first three features are observable in the X-ray band (e.g., M86 and M49 in Virgo, Forman et al. 1979, Irwin & Sarazin 1996, respectively). The bow shock is generally too faint even if favorably oriented.

Chandra and XMM-Newton observations have now reached a quality to reveal the details of the gas removal process and a wealth of structures: M89 in the Virgo cluster has a curved tail and two 'horns' attached to its upstream edge, bending downstream (Machacek et al. 2006). M86 in Virgo shows a spectacular 150 kpc long bifurcating tail starting in a plume (Randall et al. 2008), M49 in Virgo (Kraft et al. 2011) has a ragged upstream edge and a flaring tail, M60 in Virgo has a pair of double wings and only a faint tail (Wood et al., submitted), and the tail of NGC 1404 in Fornax appears rather faint despite its projected proximity to the cluster center (Machacek et al. 2005). The details and differences of the gas-stripped cluster ellipticals intriguingly suggest the opportunity to determine the still ill-constrained ICM transport properties (thermal conductivity and viscosity) and the structure of magnetic fields in the ICM because these ICM plasma properties shape the flows in and around the stripped galaxies.

The patterns of viscous and inviscid flows around solid bodies are well-known. Recall, e.g., the flow past a cir-

eroediger@hs.uni-hamburg.de
[5] Visiting Scientist, SAO

cular cylinder or sphere (van Dyke 1982, among others): From high to low viscosity, or from low to high Reynolds number[2], flow patterns change from laminar to a downstream vortex pair or torus to a turbulent wake.

The ICM flow past the atmosphere of an elliptical galaxy should behave similarly, and the observed structure of a stripped atmosphere and its wake should trace these flow patterns. The most obvious feature should be the structure of the wake: In a turbulent wake the stripped gas should mix quickly with the ambient ICM, reducing the gas density and hence X-ray brightness. A sufficient viscosity or aligned magnetic field suppresses Kelvin-Helmholtz instabilities (KHIs, Roediger et al. 2013, Chandrasekhar 1961), which are a major agent of turbulent mixing. Therefore, in a sufficiently viscous or magnetized ICM, we expect an unmixed, cool, X-ray bright tail.

However, atmospheres of elliptical galaxies are not solid bodies. Instead, the atmospheres are compressible, bound by the galactic potential, and decrease in size with time due to the ongoing stripping. The ICM flow past the galaxy is not steady but varies in velocity and density along the galaxy's orbit through the cluster. In this first paper of a series, we identify characteristic stages and flow patterns around and inside elliptical galaxies undergoing inviscid gas-stripping. We do so by simulating an elliptical, or rather spherical, galaxy during cluster crossing as described in Sect. 2. To facilitate the most direct comparison to observations, the simulations presented here are tailored to the stripped Virgo elliptical M89 regarding gravitational potential, gas contents, and orbit as described in App. A. The qualitative results are, however, independent of the exact galaxy model. In Sect. 3 we describe flow patterns and their evolution, relate flow patterns in galaxy stripping to flow patterns around solid bodies, and suggest a consistent terminology. In Sect. 4 we briefly compare our results to previous work and discuss implications. Section 5 summarizes our results. In paper II of this series (Roediger et al.) we investigate the impact of an isotropic ICM viscosity on the stripping process and present observable signatures of viscous and inviscid stripping. A detailed analysis of new M89 Chandra and archival XMM data is presented in paper III (Kraft et al.), along with a comparison to the viscous and inviscid simulations.

2. METHOD

We model the motion of a spherical galaxy through its host cluster with 3D hydrodynamic simulations. The simulations are run in the rest frame of the galaxy, i.e., the galaxy is exposed to an ICM head wind which varies in density and velocity according to the galaxy's orbit though the host cluster. We neglect gradients in the Virgo ICM and potential perpendicular to M89's orbit, and treat M89's gravitational potential as static. At a pericenter distance of $\geq 350\,\mathrm{kpc}$, M89's tidal stripping radius due to the Virgo cluster potential is $\sim 100\,\mathrm{kpc}$, much larger than the size of the remnant atmosphere. Thus, tidal effects due to the cluster potential are unimportant for M89. They may play a role for galaxies plunging deeper into their host potentials.

The model galaxy consists of an analytic gravitational potential due to its dark matter and stellar contents, and an initially hydrostatic $\sim 0.4\,\mathrm{keV}$ hot atmosphere. The model galaxies used here are tailored to the Virgo elliptical M89 as described in App. A. However, we tested a variety of galaxy models and found the flow patterns described below to be generic.

Stellar mass loss in elliptical galaxies is expected to replenish the galactic atmosphere. Mathews (1989) give a rate of $5.4 \times 10^{-20}\ \mathrm{s}^{-1}\rho_*$ for an old stellar population, where ρ_* is the spatial stellar density distribution. This corresponds to a total replenishment rate of $3.4 \times 10^8 M_\odot$ per Gyr for our M89 model. If replenishment could proceed undisturbed for 1 Gyr, the replenished gas mass would exceed the pre-existing one only in the central 4 kpc of M89, i.e., inside its current stripping radius. Hence the initially pre-existing atmosphere dominates the stripping features during first infall, and we neglect replenishment by stellar mass loss. Lu & Wang (2011) study a replenishment-only case in a constant ICM wind.

We model both the galactic atmosphere and the ICM as inviscid gases with an ideal equation of state. Thermal conduction and viscosity are neglected. The effect of viscosity is investigated in paper II. We do not include radiative cooling or AGN heating of the galactic gas but assume that thermal balance is maintained by the interplay between both.

2.1. *Code*

We use the FLASH code (version 4.0.1, Dubey et al. 2009), a modular, block-structured AMR code, parallelized using the Message Passing Interface library. It solves the Riemann problem on a Cartesian grid using the Piecewise-Parabolic Method.

The size of our simulation box is $(-400\,\mathrm{kpc}, 400\,\mathrm{kpc})^3$, sufficiently large to capture the impact of the galaxy's potential on the ambient ICM. The galaxy is centered in the simulation box. The ICM wind enters along the x-axis. The upstream boundary is an inflow boundary, where ICM density and temperature vary according to the current position of the upstream boundary in the cluster. The inflow velocity equals the opposite of the galaxy's current orbital velocity. The downstream boundary is an open boundary except for the outflow velocity being set equal to the inflow velocity. This ensures a correct ICM wind also in the subsonic regime. The side boundaries are open. ICM loss through them is negligible due to their large distance to the galaxy.

FLASH offers adaptive mesh refinement on various conditions. We wish to resolve the galactic atmosphere and its removal and subsequent mixing with the ICM in the wake. As turbulence tends to be volume-filling, any useful refinement criteria would lead to refining the complete wake region. We therefore use a fixed nested refinement around the galaxy and its tail, with a peak resolution of 0.1 kpc. The peak resolution is ensured in the box of at least $(-10\,\mathrm{kpc}, 22\,\mathrm{kpc}) \times (\pm 10\,\mathrm{kpc})^2$ around the galaxy center. At late times the upstream extent of the peak resolution box is reduced to $\sim 2\,\mathrm{kpc}$ beyond the remnant atmosphere. The peak resolution region thus fully encompasses the remnant atmosphere at pericenter passage. The volume resolved to 0.2 kpc always encompasses the whole atmosphere and the downstream

[2] The Reynolds number is defined as $\mathrm{Re} = \frac{lv\rho}{\mu}$ where l and v are the characteristic length scale and velocity of the flow, and ρ and μ are the fluid density and dynamic viscosity.

deadwater region up to at least $\sim 45\,\mathrm{kpc}$ from the galaxy center. We confirmed that the resolution is sufficient for convergence of our results (see Fig. 16 in paper II).

2.2. *Seeding instabilities*

Instabilities grow from perturbations. We do not rely on seeding the instabilities by the numerical discretization, but introduce intentional seeds by repeatedly adding small perturbations to the ICM wind velocity in x-direction. The perturbation is a uniform superposition of sinusoidal waves of wave lengths 32, 16, 8, ..., 1 kpc, covering the size range from the initial atmosphere down to below the final stripped atmosphere. We chose a total amplitude of $50\,\mathrm{km\,s^{-1}}$ (few percent of sound speed) per perturbation event. These perturbations are added every 300 Myr as they move out of the simulation box with the ICM wind. While our perturbations are highly idealized in their power spectrum and direction, they serve the purpose of seeds for the KHI and mixing. Similar to Shin & Ruszkowski (2013), we find that including perturbations enhances the gas removal rate. At the level of perturbations used here it is a secondary effect, though.

2.3. *Simulation runs*

Galaxy models and orbits are described in detail in App. A. Here we discuss the following simulation runs, sampling the uncertainty of M89's initial atmosphere and orbital velocity:

- galaxy with compact initial gas atmosphere ($n \propto r^{-1.5}$) on the slow orbit (pericenter velocity $1050\,\mathrm{km\,s^{-1}}$ =Mach 1.3),
- galaxy with extended initial atmosphere ($n \propto r^{-1.2}$) on the fast orbit (pericenter velocity $1350\,\mathrm{km\,s^{-1}}$ =Mach 1.7).

The inner atmosphere for both galaxy models agrees with the one observed in M89. In all cases the pericenter distance of the orbit is 350 kpc, equal to M89's projected distance to the Virgo center, which is very likely similar to the true cluster-centric distance as argued in paper III (see also App. A.2.1).

The simulations start at a generous spatial and temporal distance of $\geq 0.8\,\mathrm{Mpc}$ and $\geq 1\,\mathrm{Gyr}$ prior to the galaxy's pericenter passage, and always with a subsonic initial ICM flow. This ensures that the stripping can reach a quasi-equilibrium state.

3. FLOW PATTERNS AND THEIR EVOLUTION

Figure 1 shows the evolution of gas stripping of the initially compact atmosphere during the galaxy's infall into the Virgo cluster. The figure covers the evolution from 1 Gyr prior to pericenter passage to 120 Myr after pericenter passage. As known from previous work, the galactic atmosphere is stripped to successively smaller radii as the ICM flow around it gets denser and faster. Stripped-off gas is eventually carried away by the ICM flow.

The goal of this paper is to determine the flow patterns and structure in and around the stripped galactic atmosphere. In the discussion below we distinguish between the flow of the ICM *around* the galactic remaining atmosphere on the one hand and the evolution of the atmosphere on the other hand. It is also instructive to compare to the flow around solid bodies, which we do in Fig. 2 and Sect. 3.2. Occasionally the term 'remnant merger core' has been used for gas-stripped atmospheres of galaxy groups or galaxies. Here we focus on the gas stripping instead of gravitational, merger-related effects, and will therefore refer to the stripped atmosphere as 'remainng' or 'remnant' atmosphere. Furthermore, we will show below that the remnant atmosphere can have a pronounced elongated shape which is not well-described by the term 'core'.

It is well-known from experiments that an impulsive onset of a flow around a solid body is followed by a relaxation phase that lasts several object crossing times (=length/velocity) before the flow settles into a quasi-equilibrium state. During a galaxy's cluster passage, the ICM head wind varies in density and velocity by a factor of several in both quantities. The ram pressure in the simulated part of M89's orbit varies by a factor of ~ 50. Consequently, the radius of the atmosphere shrinks dramatically due to gas stripping. As both ambient wind and object size vary, we expect – and find – an extended relaxation phase for galaxy stripping. The left and right columns in Fig. 1 show the relaxation phase and the quasi-equilibrium phase, respectively. We describe both phases in more detail below.

The further goal of this series of papers is to study the effects of ICM plasma properties. To allow direct comparison of the impact of different dynamical conditions (here compact or extended atmosphere) and ICM properties (here viscosity), we show a side-by-side comparison of snapshots from inviscid and viscous simulations in Fig. 3. For details of the viscous stripping please refer to paper II.

3.1. *Evolution of the remnant atmosphere*

The ambient ICM flow strips and deforms the galaxy's atmosphere in characteristically different manners at the atmosphere's upstream part, its sides, and its downstream part. These flow regions are labelled in the middle and bottom panel in Fig. 2. Below we discuss these flow regions separately.

3.1.1. *Evolution of upstream atmosphere*

The pressure in the galactic atmosphere increases towards the galactic center, and the ICM ram pressure cannot push back gas from the central region where the galactic pressure exceeds the ram pressure. Thus, the ICM ram pressure pushes the upstream atmosphere back to the radius where the ICM ram pressure is balanced by the thermal pressure in the atmosphere (see pressure slices in Fig. 3, also Mori & Burkert 2000). This allows to estimate the upstream stripping radius as shown in Figs. 4 and 7.

After the onset of the flow, this pressure balance is reached quickly, within 100 Myr (Figs. 1, 4, also Figs. 6 and 7 for the extended atmosphere). As both ICM thermal and ram pressure increase during the galaxy infall, the upstream radius of the remnant atmosphere continues to decrease slowly up to pericenter passage (Figs. 4, 7). In all our simulations, the final upstream radius is similar to the observed value for M89, which is a sim-

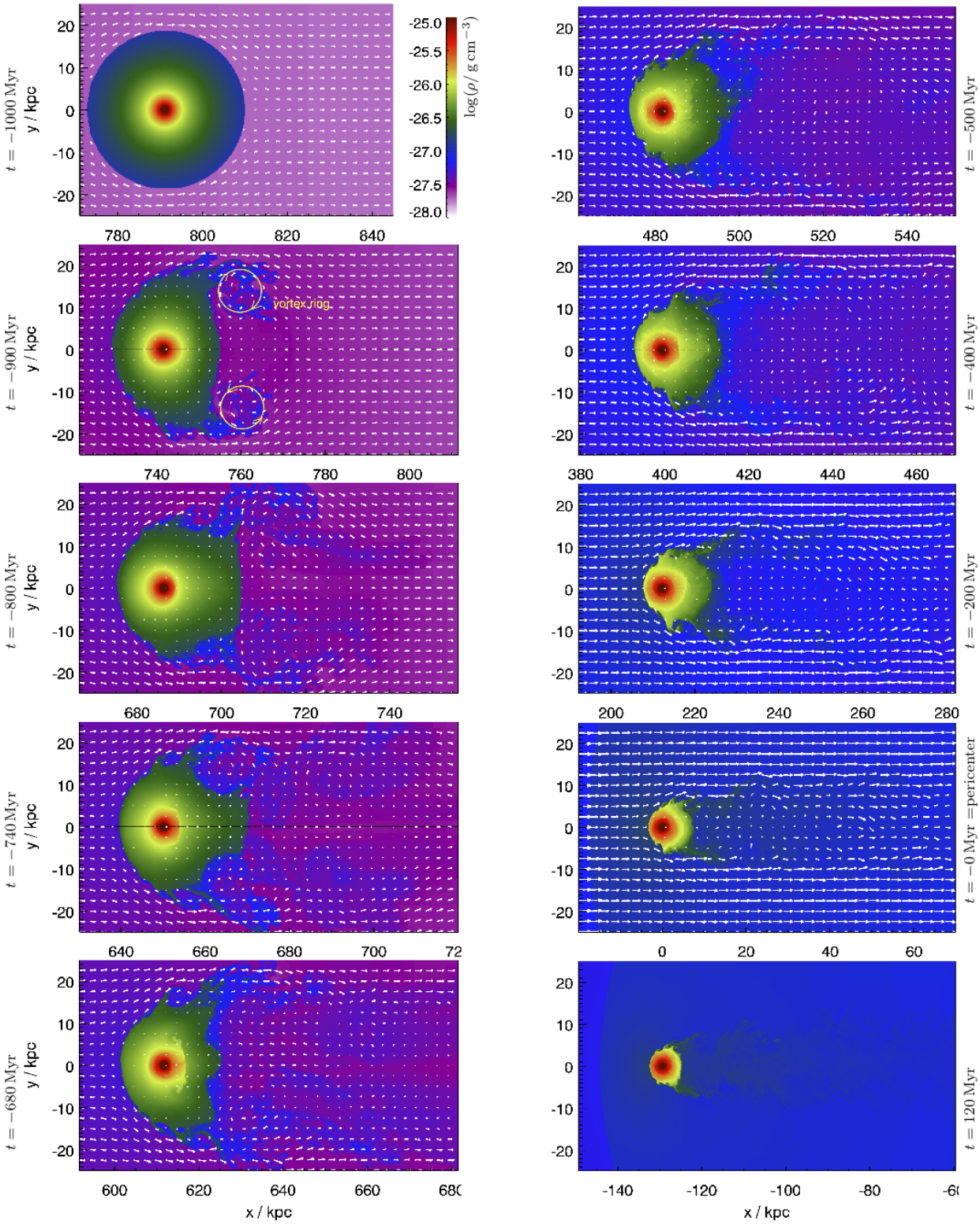

Figure 1. Inviscid stripping of spherical galaxy with initially compact atmosphere. Density slices through the galaxy in the orbital plane, overlaid with velocity vectors (except last panel). The x-axis denotes the distance to pericenter. The left column shows the initial relaxation phase (Sect. 3). After the onset of the ambient flow, a vortex ring forms as marked in the second panel, and the downstream atmosphere oscillates back and forth twice. In the quasi-equilibrium phase (right column), the flow patterns remain constant qualitatively, but their spatial scale decreases due to the ongoing stripping. The downstream atmosphere is shielded from the ICM flow and can be retained up to pericenter passage. Fig. 2 contains a snapshot with flow structures labelled. Throughout the evolution, the upstream edge is pushed back, and KHIs remove gas from the sides of the galactic atmosphere. Fig. 4 shows the evolution of the atmosphere's radius towards the upstream, downstream, and side direction.

flow around a solid sphere:

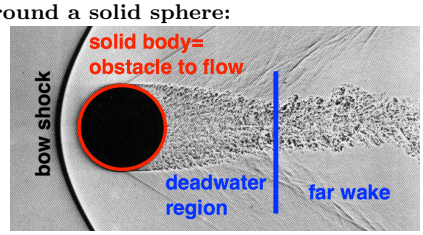

flow around a stripped spherical galaxy, density of initial atmosphere $\propto r^{-1.5}$:

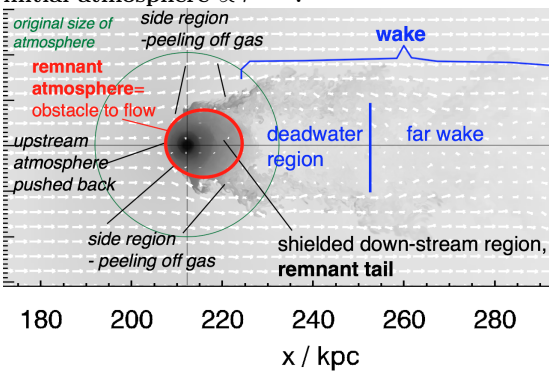

flow around a stripped spherical galaxy, density of initial atmosphere $\propto r^{-1.2}$:

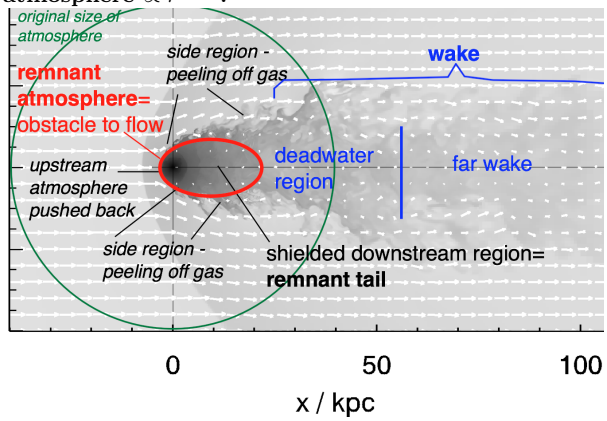

Figure 2. Comparison of flow patterns around a solid body and in elliptical galaxy stripping. We label flow regions in the ambient gas in blue and in the galactic atmosphere in black, see Sect. 3.
Top: Schlieren photo of supersonic flow around a solid sphere in air, flow regions labelled (Mach 1.5, Re $\sim 4.4 \times 10^5$; Fig. 266 from van Dyke 1982, photo by A.C. Charters).
Middle and bottom: Slice through an inviscidly stripped spherical galaxy, gas density shown in grey-scale, velocity vectors overlaid. The green circle marks the initial extent of the galaxy's atmosphere. The center of the galactic potential is marked with the crosshair. The middle panel is for the initially compact atmosphere at 200 Myr (212 kpc) prior to pericenter passage, moving with Mach 1.1; the bow shock just starts forming at $x \approx 180$ kpc and is still very faint. The bottom panel is for the initially extended atmosphere at pericenter passage, moving with Mach 1.7; the bow shock is clearly visible.
Qualitatively, flow patterns around the solid sphere and *around* the stripped atmospheres are very similar. The stripped atmospheres retain a remnant tail that is part of the remnant atmosphere. The extent of the current atmosphere is marked by the red ellipse. The whole atmosphere including the remnant tail poses the obstacle to the ambient ICM flow as does the solid body in the top panel. The remnant tail is longer for an initially extended atmosphere. The longer remnant tail leads to a longer deadwater region as well.

ple consequence of tailoring the galactic potential, inner atmosphere and ICM wind to this galaxy.

3.1.2. *Evolution of the sides of the atmosphere*

The actual gas removal occurs along the sides of the galactic atmosphere where the shear flow, with respect to the ICM, is largest (Fig. 1). In these inviscid simulations, KHIs transfer momentum into the outer layers and thus ablate gas from the sides of the atmosphere. The atmosphere's radius to the sides, i.e., perpendicular to the galaxy's direction of motion, is typically 1.5 times larger than the upstream radius (Fig. 4, 7). This gas removal mechanism is always present, it starts immediately after onset of the ICM wind and continues past pericenter passage (see also Nulsen 1982).

3.1.3. *Evolution of the downstream atmosphere*

The downstream part of the atmosphere evolves differently during the initial relaxation phase and during quasi-steady stripping. After the onset of the ICM wind the downstream ICM develops an initial vortex ring (Fig. 1, left panel in second row). The same flow pattern occurs shortly after the onset of a flow past a solid object (see Fig. 59 in van Dyke 1982, or Fig. 5.11.3 in Batchelor 2000, taken from Prandtl 1927). Simultaneously, stripped galactic gas is pulled into the downstream ICM. Subsequently, in shedding this first vortex ring, downstream pressure decrements and backflows alternately pull and push the downstream atmosphere. Being compressible, it adapts to these transitions by a series of two to three oscillations as shown in the evolution snapshots in Fig. 1 and clearly evident in the evolution of the downstream radius in Fig. 4. This initial relaxation phase lasts for several 100 Myr due to the ongoing increase of the ICM wind and shrinking of the atmosphere.

At about 500 Myr prior to pericenter passage, the flow reaches a quasi-equilibrium state (Fig. 1). Now a wake is established downstream of the galaxy, and oscillations of the downstream atmosphere occur only at a small amplitude (Fig. 4). The downstream part of the remnant atmosphere is shielded from the ICM wind. Consequently, gas loss from the downstream side is very slow, and much of the downstream atmosphere can survive up to or even beyond pericenter passage. Thus, the remnant atmosphere is distinctly asymmetric, extending farther downstream than upstream. The longer downstream part can even have the visual appearance of a tail, especially for initially more extended galactic atmospheres (see Sect. 3.3 and Fig. 6). We refer to this elongated unstripped downstream part of the atmosphere as the 'remnant tail'. The gas fraction slices in Fig. 3 clearly show that the remnant tail consists almost exclusively of galactic gas, i.e., it is not mixed. The remnant tail is part of the 'obstacle' the atmosphere poses to the ICM flow. Thus, the analogy to the flow past a solid body should not use a sphere but an elongated body.

3.1.4. *Evolution of the atmosphere after pericenter passage*

After pericenter passage, the ICM wind decreases and the upstream radius remains approximately constant. Gas removal along the sides continues, and finally the slow downstream stripping by the downstream backwards flow in the deadwater region (see Sect. 3.2) catches

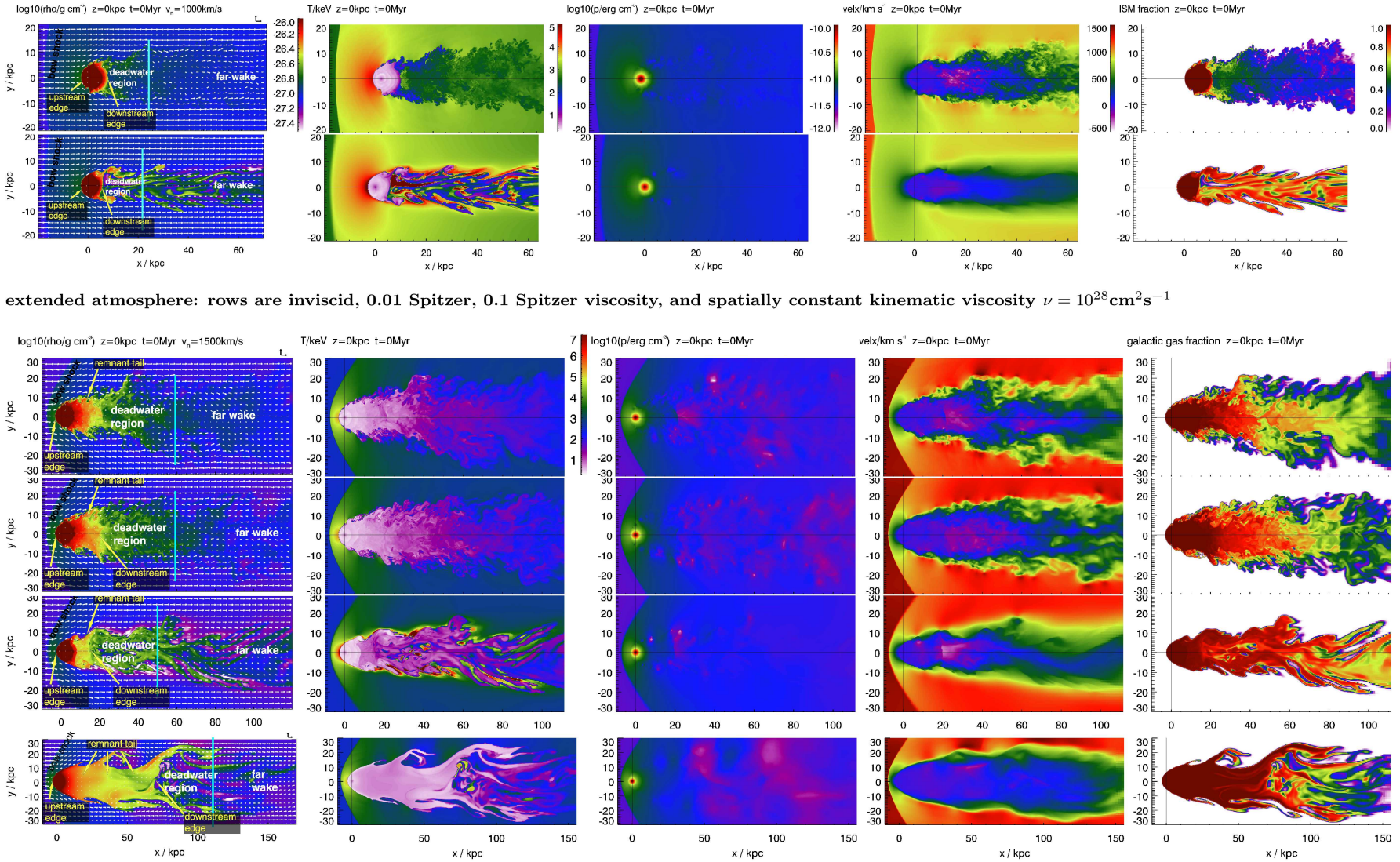

Figure 3. Comparison of flow patterns of a stripped spherical galaxy; type of galaxy atmosphere and ICM viscosity as labelled. The panels show slices through the 3D simulation box, color-coding the gas density, temperature, pressure, velocity along the orbit, and galactic gas fraction from left to right. The galactic center is at $(0, 0)$ in all panels. In the left column velocity vectors are overlaid and flow patterns labelled. Global flow patterns are the same in all cases, but the position and size of the deadwater region depends on the length of the remnant atmosphere. Viscosity determines the mixing in the deadwater region and far wake. Note the different length scales between different rows. See Sect. 3 in this paper and Sect. 3 in paper II for details.

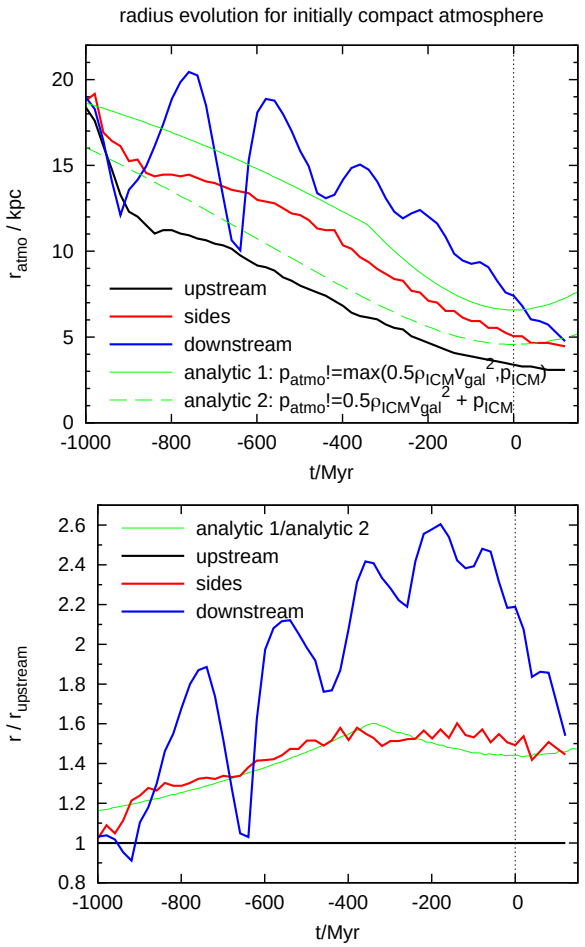

Figure 4. Evolution of the size of the remnant atmosphere measured[a] towards the upstream and downstream direction and towards the sides for the initially compact atmosphere (see Fig. 1). The top panel plots the radii in these three direction in kpc, the bottom panel is normalized to the upstream radius. In green, two versions of an analytic estimate of the stripping radius are shown: The stripping radius is estimated where the atmosphere's pressure $p_{\rm atmo}$ equals the maximum of ICM ram pressure, $0.5\rho_{\rm ICM}v^2_{\rm ICM}$, and thermal pressure, $p_{\rm ICM}$, or their sum. These analytic estimates closely follow the trends for the side radius and upstream radius, but slightly over-predict them. The downstream radius first experiences strong oscillations, then remains significantly larger than the upstream and side radii until pericenter passage.

[a]To measure the atmosphere's radius we take entropy profiles in 20^o cones/slices towards each direction. Gas with entropy below 50 keV cm^2 is defined as galactic gas.

up and erodes the remnant tail. Otherwise, flow patterns remain as described for the quasi-equilibrium phase above.

3.1.5. *Flow inside the atmosphere*

The galaxy's atmosphere is gaseous itself. Instead of the flow around a solid body, the scenario of a drop of heavier fluid falling through a lighter fluid could be a closer terrestrial analogue. At the sides of such a drop, either KHIs or viscosity transfer momentum into the drop, pulling its outer layers into the downstream direction. In turn, a vortex-like flow is established inside the drop, such that the inner part of the drop moves towards the upstream interface. In the long run, the initially spherical drop turns into a cap-shape and a ring, which eventually breaks apart due to Rayleigh-Taylor instabilities (assuming sufficiently low surface tension).

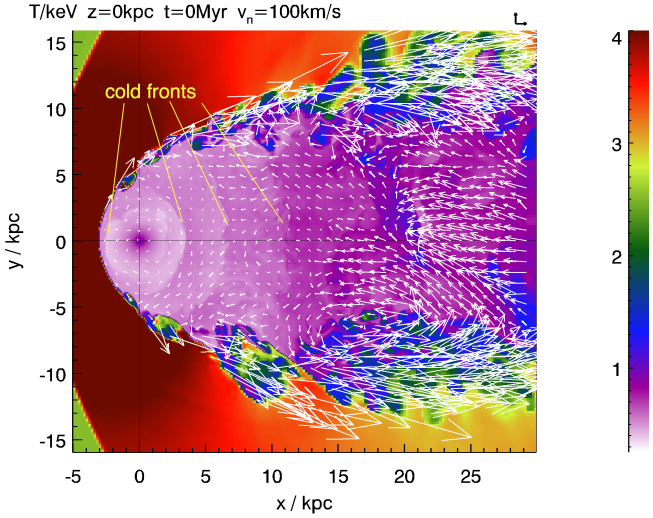

Figure 5. Flow patterns inside the remnant atmosphere: Temperature slice through the atmosphere (initially extended atmosphere, inviscid) at pericenter passage. We overplot velocity vectors where the galactic gas fraction exceeds 0.3. Sloshing of the atmosphere leads to sloshing cold fronts. Turbulent motions are superimposed to the sloshing.

A similar pattern could be expected in the atmosphere of the stripped galaxy, but never occurs in our simulations. Instead, after the onset of the ICM wind, a vortex ring is formed in the *downstream* galactic gas or in the downstream ICM (Figs. 1 and 6, left panels in second or first row, respectively). This vortex ring does not transport gas to the upstream edge of the atmosphere because its ram pressure is too weak to displace the dense central gas peak from the deep central potential well. For shallow central gravitational and gas density gradients this could be possible (e.g., in the simulations of Heinz et al. 2003), and may be observed in the cluster Abell 115 (Forman et al. 2014).

Instead of a drop-like flow, the initial push by the onset of ICM flow leads to a series of long-lived sloshing motions of the atmosphere. These are superimposed with the stripping dynamics described above. The internal sloshing leads to a series of weak density and temperature discontinuities inside the atmosphere (Fig. 5), which are sloshing cold fronts just like their counterparts seen in minor cluster mergers (e.g., Markevitch & Vikhlinin 2007, Roediger et al. 2012). The sloshing cold fronts in the upstream part of the atmosphere are stripped by the ICM wind, but remain intact in the remnant tail. These internal cold fronts are superimposed with irregular motions of a few ten km s^{-1}.

3.2. *Flow around the remnant atmosphere*

The ICM flow around the remnant atmosphere resembles the flow past a solid body in the initial relaxation phase as well as in the quasi-steady phase (Fig. 2). In case of a solid body, the relaxation phase after an impulsive onset of the flow proceeds in a characteristic series of stages: Right after the onset the flow appears laminar. Next, a downstream vortex ring forms. Then the wake starts shedding vortices or turns turbulent for sufficiently large Reynolds numbers (see Fig. 59 in van Dyke 1982, or

Fig. 5.11.3 in Batchelor 2000 (taken from Prandtl 1927). Similar patterns are seen for galaxy stripping in the left columns of Figs. 1 and 6.

In the quasi-steady state, the flow past a solid body leads to a wake downstream of the body (top panel of Fig. 2). The near wake, i.e., the region immediately downstream of the body, is a 'backflow' or 'dead-water' region, where the average gas velocity is very slow and directed upstream (in the rest frame of the body). Such deadwater regions are obvious in the wakes of cars or trucks – they can drag along dust or dry leaves behind them. In the far wake the mean gas flow is directed away from the moving body.

In quasi-steady stripping, the ICM flow past the remnant atmosphere leads to a very similar wake (Fig. 2) including a deadwater region as clearly evident from the velocity vectors in Fig. 1. The deadwater region is generally about 1.5 times as long as the total length of the remnant atmosphere, in qualitative agreement with laboratory results for solid spheres (Taneda 1956a). The wake of a supersonic solid body is usually about as wide as the cross-section of the body. The wake of a stripped galaxy tends to be somewhat wider than the remnant atmosphere because the atmosphere itself is continuously shrinking. The galaxy's wake is in pressure equilibrium with the ambient ICM except for scattered low-pressure regions inside vortices. The backwards flow in the near wake leads to a downstream contact discontinuity that marks the downstream end of the remnant tail.

The wake of a stripped galaxy is of particular interest because galactic gas stripped from the atmosphere is transported into the wake and traces the wake closely. Here, stripped-off galactic gas could potentially mix with the ICM unless the mixing is prevented by ICM viscosity or magnetic fields (see galactic gas fraction panels in Fig. 3). Stripped gas could also be trapped in the deadwater region for an extended time, in analogy to the dust behind a moving truck. Thus mixing in the deadwater region will depend on the amount of trapped galactic gas as well. Only stripped gas that reaches the far wake can be transported away from the galaxy.

For solid spheres, a deadwater region exists unless the fluid has a very low Reynolds number ($\lesssim 24$, Taneda 1956a). It can extend as far as one or more body lengths downstream of the body (Taneda 1956a). At moderate Reynolds numbers around 100, the deadwater region takes the shape of a vortex ring or vortex pair in 3D and 2D, respectively (e.g., Taneda 1956a,b, see also Fig. 13 in paper II). Stripped gas trapped in the smooth flow of a vortex ring should not mix efficiently with the ICM. In the far wake vortices are shed, which, in 2D, form the von Karman vortex street. At Reynolds numbers above ~ 1000 both deadwater region and far wake are turbulent as shown in Fig. 2. In paper II we show that the global flow patterns discussed here also exist in viscous stripping, but mixing in the wake is indeed suppressed (see Fig. 3).

If moving supersonically, both solid bodies and stripped galaxies cause an upstream bow shock.

3.3. *Initially compact vs. extended galactic atmosphere*

Figure 6 displays snapshots of the stripping of an initially extended atmosphere (galactic gas density $\propto r^{-1.2}$ instead of $\propto r^{-1.5}$). The left and right columns show the initial relaxation phase and the quasi-equilibrium phase, respectively. Fig. 7 summarizes the size evolution of this atmosphere. The bottom panel of Figure 2 shows a labelled density slice from this simulation for direct comparison to the compact atmosphere and the flow around a solid sphere. Qualitatively the stripping proceeds in the same manner as described above.

A more extended initial atmosphere leads to a longer relaxation phase after flow onset, in the case shown here it lasts almost 1 Gyr. As we simulated this galaxy on the orbit with a faster pericenter velocity, this simulation started 1.5 Gyr prior to pericenter passage to ensure a subsonic flow onset. Also here stripping reaches a quasi-equilibrium about 0.5 Gyr prior to pericenter passage.

Second, an initially more extended atmosphere retains a longer downstream atmosphere – or remnant tail – for a longer time because, as explained above, the downstream atmosphere is shaded from the ICM wind and downstream stripping is very slow. In the case presented here the remnant tail survives until 300 Myr (390 kpc) after pericenter passage, and it can be 6 to 9 times longer than the upstream radius. Despite this length, the remnant tail contains unstripped, unmixed galactic gas just as for the compact atmosphere.

For either atmospheres, the deadwater region starts only downstream of the remnant tail and is typically 1.5 times as long as the total length of the remnant atmosphere including the remnant tail. For the extended atmosphere, turbulence in the deadwater region and slow turbulence inside the remnant tail somewhat blur the downstream contact discontinuity between these two flow regions. In case of the initially extended atmosphere, the combination of the longer remnant tail, the longer deadwater region, and the initially more extended galactic atmosphere lead to more galactic gas being trapped in the deadwater region.

4. DISCUSSION

Our simulations reproduce the basic features of elliptical galaxy stripping found by previous authors, i.e., the bow shock, upstream contact discontinuity and downstream tail (e.g., Acreman et al. 2003; Stevens et al. 1999; Toniazzo & Schindler 2001). Going beyond previous work, we compared the flow patterns arising in galaxy stripping to the flows around solid bodies. In this course, we distinguished the remnant tail of the atmosphere and the galaxy's wake, which had been summed up into the term 'tail' before. These flow patterns can be seen in snapshots presented in earlier work (e.g., Acreman et al. 2003; Stevens et al. 1999), but their origin and implications have, to our knowledge, not been discussed. Distinguishing between the remnant tail and the wake is important because only in the latter can mixing between stripped galactic gas and ICM take place. The remnant tail always contains pure galactic gas only, and thus cannot be used as a tracer of ongoing or suppressed mixing. Shin & Ruszkowski (2013) argue that a sufficient level of turbulence inside the galactic atmosphere can lead to diluting the galactic atmosphere with ICM over a timescale of Gyrs. However, their study does not include a realistic stripping history. Given the long dilution timescale, the effect might be small in a realistic case.

Furthermore, we discussed the origin and duration of the flow initialization phase where stripping has not yet

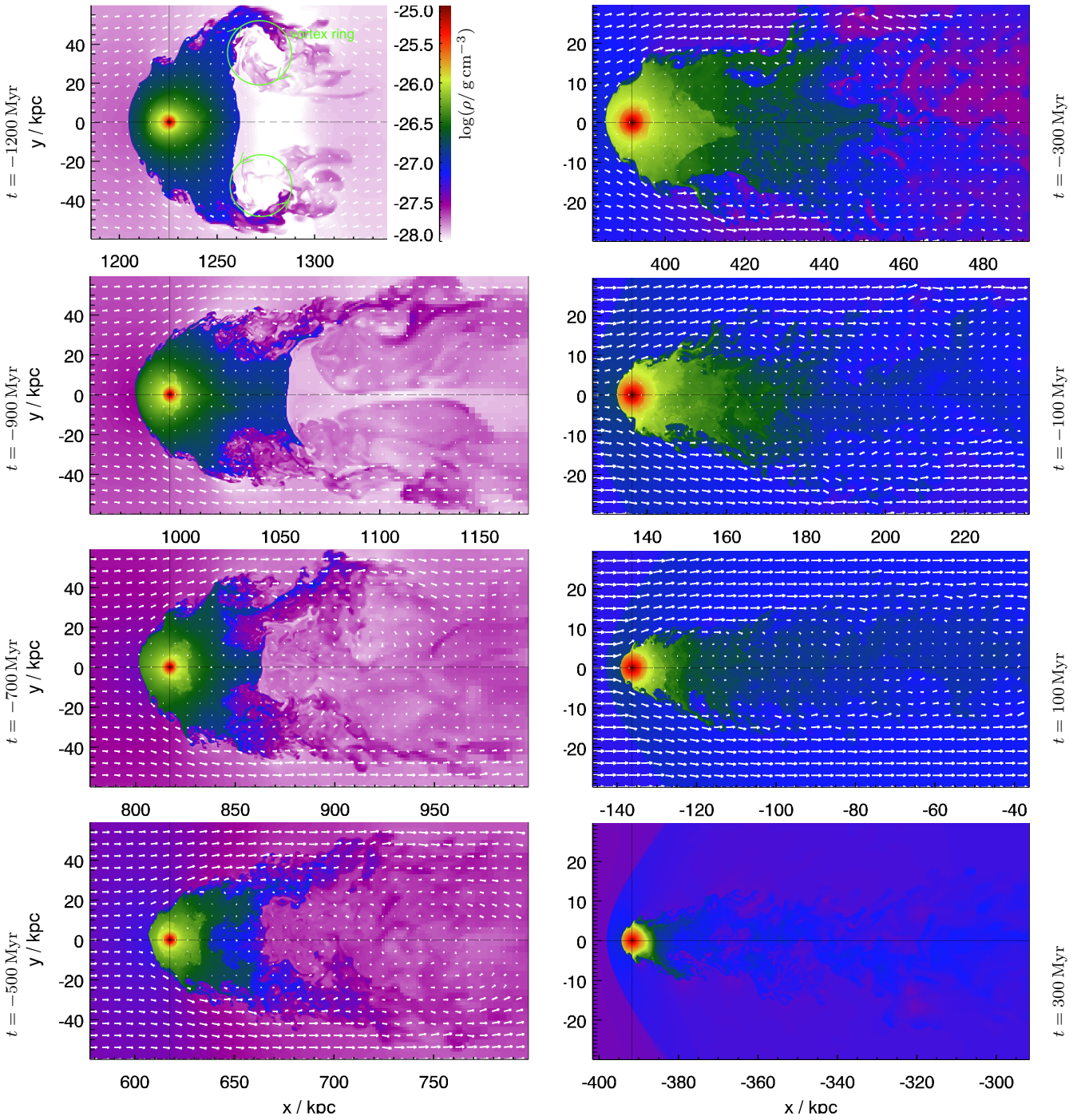

Figure 6. Inviscid stripping of initially extended atmosphere (Sect. 3.3). Density slices through galaxy in orbital plane with velocity vectors overlaid in most panels. The left column shows the initial relaxation phase, the right column the quasi-equilibrium flow. The simulation was started 1.5 Gyr (1.4 Mpc) prior to pericenter passage. The initial oscillations last almost a Gyr. The galaxy retains much of its downstream atmosphere up to pericenter passage, giving rise to a pronounced remnant tail. Only ~ 300 Myr after pericenter passage is the remnant tail eroded.

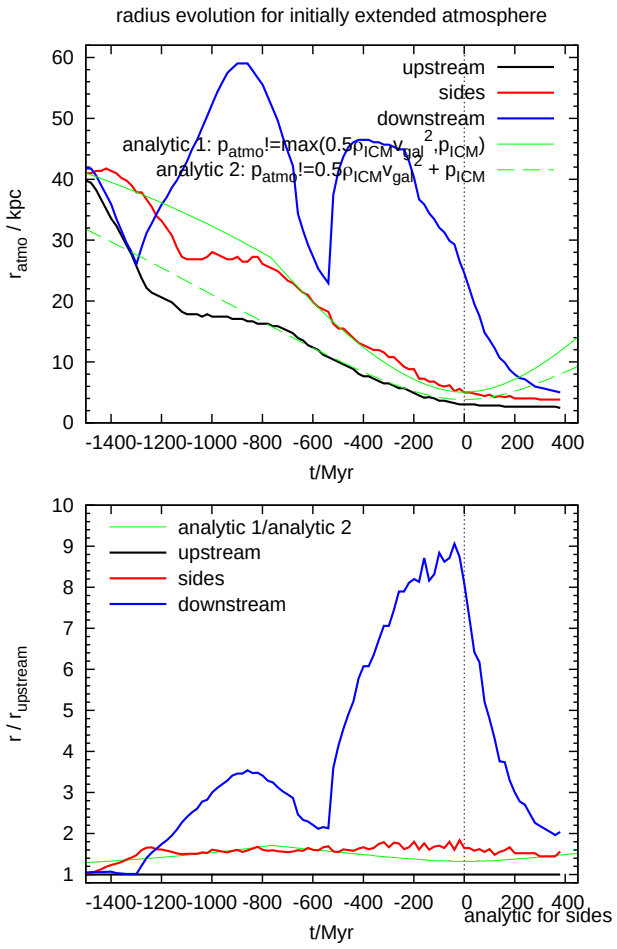

Figure 7. Evolution of the size of the remnant atmosphere towards the upstream and downstream direction and towards the sides for the initially extended atmosphere (see Fig. 6 for snapshots). Otherwise same as Fig. 4. Note the stronger downstream oscillations and the greater extent of the downstream atmosphere.

reached a quasi-steady state and the gas tail structure is still dominated by initial conditions. We demonstrated the long-lasting impact of the initial gas galactic contents, which lasts well into the quasi-equilibrium stripping phase. Consequently, direct comparisons between generic simulations and observations of particular galaxies can be difficult and misleading. In particular, simulations that expose model galaxies or subclusters to a constant ambient wind cannot reach the quasi-equilibrium stripping. First, such a model galaxy experiences the initial relaxation phase where the downstream atmosphere oscillates, and then directly enters a stage comparable to the after-pericenter stripping where the ambient wind does not increase further. For example, the simulations of Suzuki et al. (2013) and Zavala et al. (2012) cover the initial relaxation phase only.

The long-lasting signatures of the initial atmosphere's extent combined with the long-lasting flow relaxation phase could be especially interesting for groups or galaxies in an early phase of their infall into their host cluster. Such examples include M49 in the southern outskirts of the Virgo cluster, and groups in the peripheries of the clusters Abell 2142 (Eckert et al. 2014) and Abell 85 (Kempner et al. 2002). If these groups have passed the accretion shock just recently, their appearance is likely still dominated by irregular flow patterns typical for the initial relaxation phase. For the same reasons, large galaxies falling into small clusters or groups may never reach the quasi-equilibrium phase during their first infall because in the more compact cluster atmosphere the ram pressure changes more rapidly than the galaxy can adapt to.

5. SUMMARY

We determined the similarities and differences between flows around a solid blunt body on the one hand and flows in gas-stripping of elliptical cluster galaxies on the other hand. To this end, we simulated gas-stripping of the hot atmosphere of the Virgo cluster elliptical M89 (NGC 4552), taking into account a realistic gravitational potential, initial gas contents, and orbit.

First, we distinguish two aspects of the stripping process:

- Evolution of the atmosphere: The atmosphere of an infalling spherical galaxy is pushed into the downstream direction and is stripped preferentially along its sides. The downstream part of the atmosphere is shielded from the ICM wind, and a portion of the downstream atmosphere significantly larger than at the upstream part can survive stripping up to or beyond pericenter passage. This unstripped downstream gas forms the remnant tail. Only at or after pericenter passage is this remnant tail eventually stripped.

- Flow around the atmosphere: The flow of the ICM *around* the evolving atmosphere resembles the flow around a solid body. However, the equivalent of the solid body is not a sphere or ellipse, but the complete remnant atmosphere including the remnant tail. The *wake* starts only downstream of the remnant tail. The first part of the wake is a deadwater region. Gas stripped from the galaxy traces the deadwater region and far wake.

The length and density of the remnant tail and the deadwater region increase for an initially more extended galactic atmosphere. Mixing between galactic gas and ambient ICM occurs only in the wake, but not the remnant tail. Thus, observations aiming at determining ICM plasma properties via progressing or suppressed mixing between galactic gas and the ICM must probe the *wake* sufficiently downstream of the galaxy center to avoid confusion with the remnant tail.

Second, we demonstrated that a sudden onset of stripping is followed by an extended initial relaxation phase, whose presence is also known from flows past solid bodies. Galaxies or groups being stripped in cluster outskirts likely are still in the initial relaxation phase. Only galaxies nearing their pericenter passage have reached a quasi-steady stripping phase.

Paper II of this series investigates the impact of ICM viscosity on the flow patterns and derives observable signatures of inviscid and viscous stripping. Paper III gives a detailed comparison of archival XMM and new Chandra data to the simulation results.

The FLASH code was in part developed by the DOE NNSA- ASC OASCR Flash center at the University of Chicago. E.R. acknowledges the support of the Priority Programme Physics of the ISM of the DFG (German Research Foundation), the supercomputing grants NIC 6006 and 6970 at the John-Neumann Institut at the Forschungszentrum Jülich, a visiting scientist fellowship of the Smithsonian Astrophysical Observatory, and the hospitality of the Center for Astrophysics in Cambridge. We are grateful for helpful discussions with Marcus Brüggen and Dominique Eckert.

Facilities: CXO (ASIS).

REFERENCES

Acreman, D. M., Stevens, I. R., Ponman, T. J., & Sakelliou, I. 2003, MNRAS, 341, 1333
Batchelor, G. K. 2000, An Introduction to Fluid Dynamics, cambridge edn. (Cambridge: Cambridge University Press)
Blakeslee, J. P., Jordán, A., Mei, S., et al. 2009, ApJ, 694, 556
Cappellari, M., Bacon, R., Bureau, M., et al. 2006, MNRAS, 366, 1126
Cavagnolo, K. W., Donahue, M., Voit, G. M., & Sun, M. 2009, ApJSS, 182, 12
Chandrasekhar, S. 1961, Hydrodynamic and hydromagnetic stability (Oxford: Clarendon)
Churazov, E., Forman, W. R., Vikhlinin, A., et al. 2008, MNRAS, 388, 1062
Das, P., Gerhard, O., Churazov, E., & Zhuravleva, I. 2010, MNRAS, 409, 1362
Dubey, A., Antypas, K., Ganapathy, M. K., et al. 2009, Parallel Computing, 35, 512
Eckert, D., Molendi, S., Owers, M., et al. 2014, A&A, accepted
Emsellem, E., Cappellari, M., Peletier, R. F., et al. 2004, MNRAS, 352, 721
Forman, W. R., Schwarz, J., Jones, C., Liller, W., & Fabian, A. C. 1979, ApJ, 234, L27
Forman, ., Churazov, ., Heinz, ., et al. 2014, American Astronomical Society
Gisler, G. R. 1976, A&A, 51, 137
Heinz, S., Churazov, E., Forman, W. R., Jones, C., & Briel, U. G. 2003, MNRAS, 346, 13
Hernquist, L. 1990, ApJ, 356, 359
Humphrey, P. J., Buote, D. A., Canizares, C. R., Fabian, A. C., & Miller, J. M. 2011, The Astrophysical Journal, 729, 53
Humphrey, P. J., Buote, D. A., O'Sullivan, E., & Ponman, T. J. 2012, The Astrophysical Journal, 755, 166
Irwin, J. A., & Sarazin, C. L. 1996, ApJ, 471, 683
Kempner, J. C., Sarazin, C. L., & Ricker, P. M. 2002, ApJ, 579, 236
Kormendy, J., Fisher, D. B., Cornell, M. E., & Bender, R. 2009, ApJSS, 182, 216
Kraft, R. P., Forman, W. R., Jones, C., et al. 2011, ApJ, 727, 41
Lu, Z., & Wang, Q. D. 2011, MNRAS, 413, 347
Machacek, M. E., Dosaj, A., Forman, W. R., et al. 2005, ApJ, 621, 663
Machacek, M. E., Jones, C., Forman, W. R., & Nulsen, P. E. J. 2006, ApJ, 644, 155
Markevitch, M., & Vikhlinin, A. 2007, Phys. Reports, 443, 1
Mathews, W. G. 1989, The Astronomical Journal, 97, 42
Matsushita, K., Belsole, E., Finoguenov, A., & Böhringer, H. 2002, A&A, 386, 77
McCarthy, I. G., Frenk, C. S., Font, A. S., et al. 2008, MNRAS, 383, 593
Mei, S., Blakeslee, J. P., Cote, P., et al. 2007, ApJ, 655, 144
Mori, M., & Burkert, A. 2000, ApJ, 538, 559
Napolitano, N. R. 2012, Memorie della Societa Astronomica Italiana Supplement
Nulsen, P. E. J. 1982, MNRAS, 198, 1007
Prandtl, L. 1927, Journal of the Royal Aeronautical Society, 31, 730
Randall, S. W., Nulsen, P. E. J., Forman, W. R., et al. 2008, ApJ, 688, 208
Roediger, E., Brüggen, M., Simionescu, A., et al. 2011, MNRAS, 413, 2057
Roediger, E., Kraft, R. P., Nulsen, P., et al. 2013, MNRAS, 436, 1721
Roediger, E., Lovisari, L., Dupke, R., et al. 2012, MNRAS, 420, 3632
Scharf, C. A., Zurek, D. R., & Bureau, M. 2005, ApJ, 633, 154
Schindler, S., Binggeli, B., & Böhringer, H. 1999, A&A, 343, 420
Shibata, R., Matsushita, K., Yamasaki, N. Y., et al. 2001, ApJ, 549, 228
Shin, M.-S., & Ruszkowski, M. 2013, MNRAS, 428, 804
Simionescu, A., Werner, N., Forman, W. R., et al. 2010, MNRAS, 405, 91
Stevens, I. R., Acreman, D. M., & Ponman, T. J. 1999, MNRAS, 310, 663
Suzuki, K., Ogawa, T., Matsumoto, Y., & Matsumoto, R. 2013, The Astrophysical Journal, 768
Takeda, H., Nulsen, P. E. J., & Fabian, A. C. 1984, MNRAS, 208, 261
Taneda, S. 1956a, Journal of the Physical Society of Japan, 11
—. 1956b, Journal of the Physical Society of Japan, 11
Toniazzo, T., & Schindler, S. 2001, MNRAS, 325, 509
Tonry, J. L., Dressler, A., Blakeslee, J. P., et al. 2001, ApJ, 546, 681
Urban, O., Werner, N., Simionescu, A., Allen, S. W., & Böhringer, H. 2011, MNRAS, 414, 2101
van Dyke, M. 1982, An album of fluid motion (Stanford: Parabolic Press)
Zavala, J., Balogh, M. L., Afshordi, N., & Ro, S. 2012, MNRAS, 426, 3464
Zibetti, S., & Groves, B. 2011, MNRAS, 417, 812

APPENDIX

A. TAILORING THE SIMULATIONS TO THE VIRGO ELLIPTICAL M89

A.1. *Galaxy potential and initial gas contents*

In the current work we neglect the ellipticity of M89 and model this galaxy as a spherical gravitational potential filled with an initially hydrostatic atmosphere. Stars and dark matter (DM) dominate the galaxy's mass, hence we neglect self-gravity in the gas and use a static potential. For simplicity we describe the galactic potential as a superposition of three Hernquist models (Hernquist 1990). Hernquist potentials have the advantage of a finite total mass. The gravitational potential $\Phi(r)$ and cumulative mass $M(r)$ of component i depend on the corresponding total mass M_i, scale radius a_i, and circular radius r as

$$\Phi(r) = -G\frac{M_i}{r+a_i}, \tag{A1}$$

$$M(r) = M_i\frac{r^2}{(r+a_i)^2}. \tag{A2}$$

The inner potential is known from its stellar light, the inner hot gaseous atmosphere from the Chandra observation of the remnant atmosphere. The outer potential and initial atmosphere are not directly known because M89 is already heavily gas-stripped; thus we use results for comparable non-stripped ellipticals and encompass the reasonable parameter space for M89 in two models. Figure 8 summarizes mass, potential, and gas profiles of the initial models. Table 1 lists the parameters of the galaxy models.

A.1.1. *Stellar component*

We approximate M89's stellar component with a double Hernquist model, which fits its stellar light profile (Kormendy et al. 2009) between 0.1 and 30 kpc (top left panel of Fig. 8). Scale radii and masses for the main and core stellar component are given in Table 1. There are several measures of the total stellar mass of M89. Zibetti & Groves (2011) convert the total H band luminosity of M89 to a total stellar mass of $10^{11} M_\odot$. Cappellari et al. (2006) and Emsellem et al. (2004) give stellar velocity dispersions of $250\,\mathrm{km\,s^{-1}}$, which corresponds to a virial

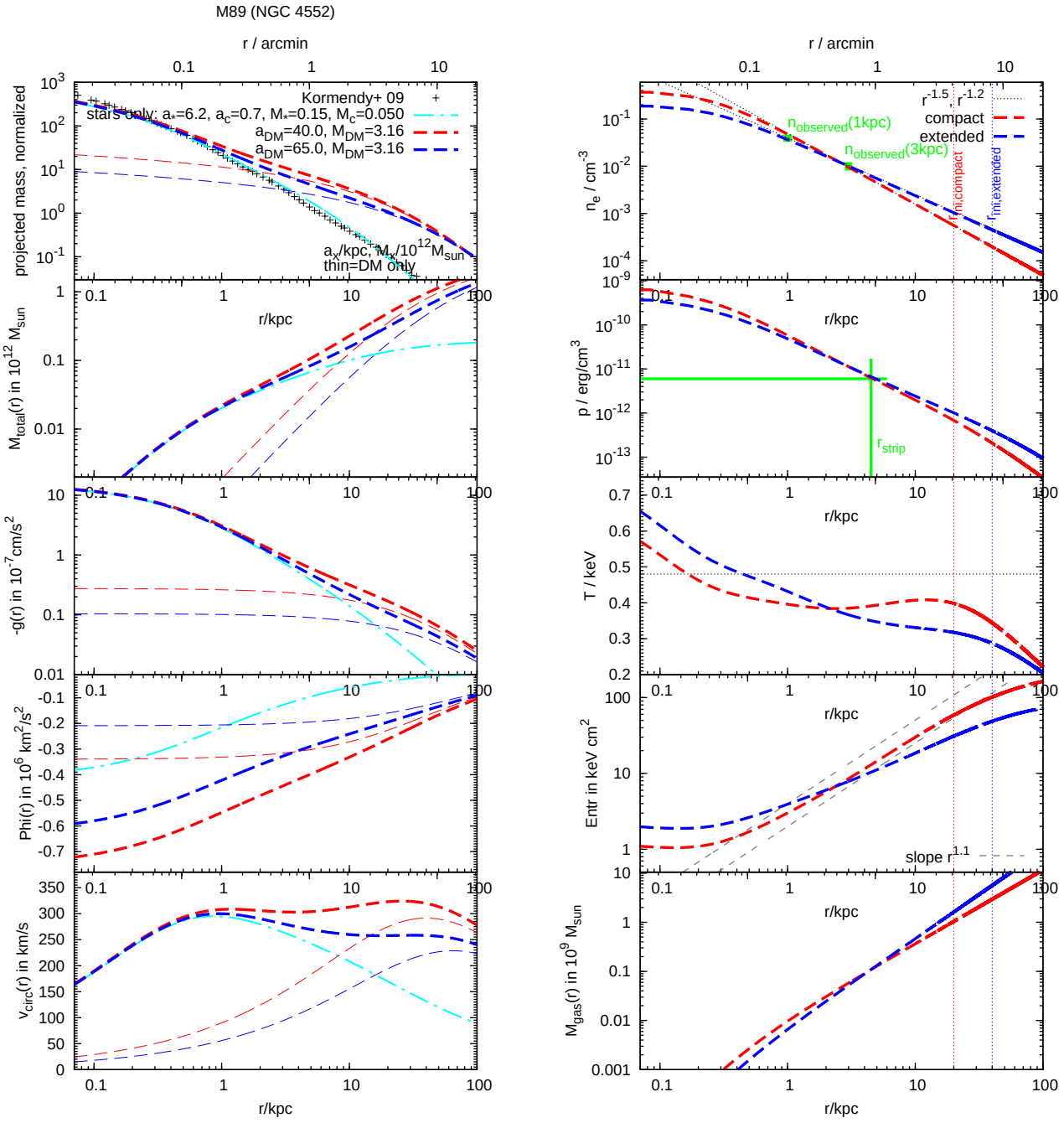

Figure 8. Model galaxy potentials (left) and galactic gas profiles (right). In the left column we plot radial profiles of projected mass and comparison to brightness profile, cumulative mass, gravitational acceleration, gravitational potential, and circular velocities. The thin lines are for the DM component only. In the right column we plot the corresponding radial profiles of electron density, thermal pressure, ICM temperature, entropy, and cumulative mass profiles. In green we mark observational constraints on the galactic atmosphere. See also App. A.1. Note that the gas profiles are relevant only out to the initial radius of the atmosphere as set by pressure balance with the initially ambient ICM (marked by thin vertical lines of matching color).

Table 1
Galaxy model parameters for M89.

stellar distribution common parameters to all models:	
$M_*/10^{11} M_\odot$	1.5
$a_*/$ kpc	6.2
$M_c/10^{11} M_\odot$	0.5
$a_c/$ kpc	0.7

DM halos and galactic atmospheres:	compact	extended
$M_{\rm DM}/10^{12} M_\odot$	3.16	3.16
$a_{\rm DM}/$ kpc	40.	65.
$n_0/\,{\rm cm}^{-3}$	0.4	0.2
$r_c/$ kpc	0.25	0.25
β	0.5	0.4
truncation radius/kpc	19	43

mass of $1.5 \times 10^{11} M_\odot$ within 10 kpc. The gaseous atmosphere of M89 is disturbed by gas stripping and a central AGN outburst. The measured gas temperature in the remnant gas core excluding the central AGN bubbles is 0.48 ± 0.03 keV (paper III). Assuming that this value is representative for the undisturbed atmosphere, this temperature corresponds to a virial mass of $3 \times 10^{11} M_\odot$ within 10 kpc radius.

A choice of $M_* = 1.5 \times 10^{11} M_\odot$ and $M_c = 0.5 \times 10^{11} M_\odot$ yields a galactic gas temperature of 0.4 keV around 3 kpc, which is still 20% below the observed temperature. However, the optical data does not support an even higher stellar mass. A lower stellar mass would reduce the gas temperature even further. M89 is currently experiencing an AGN outburst and may have been heated somewhat by earlier outbursts. Thus, the temperature of the model atmospheres agrees reasonably with the observations.

A.1.2. *Gaseous atmosphere*

Only the central part of the hot atmosphere of M89 remains, hence we extrapolate this atmosphere based on observations of other elliptical galaxies. We describe the galactic gas density profile by a β model, using $\beta = 0.5$ for a compact atmosphere (comparable to NGC 1404, Scharf et al. 2005) and $\beta = 0.4$ for a more extended atmosphere more typical for galaxy-size and group-size DM halos. We normalize the density profile to agree with the power-law fit by Machacek et al. (2006) between 1 and 3 kpc (see top right panel in Fig. 8).

We assume the initial atmosphere to be in hydrostatic equilibrium and compute the pressure and temperature profiles according to total gravitational potential. For a chosen galactic gas density, the DM potential sets the galactic gas temperature and pressure profile as described below. We assume a zero pressure at infinity and integrate the galactic atmosphere pressure profile inwards. The model galaxy is then placed at its initial position in the cluster outskirts, and its atmosphere truncated where its pressures falls below the ambient ICM pressure. The truncation radius for both models is listed in Tab. 1 and marked in Fig. 8.

A.1.3. *Dark matter (DM) halo*

The total mass of elliptical galaxies is dominated by DM albeit with considerable scatter (e.g., review by Napolitano 2012). For example, Das et al. (2010) measure DM fractions of about 80 to 90% within 4 effective radii. Thus, we expect a DM mass of roughly $2 \times 10^{12} M_\odot$ in M89. Humphrey et al. (2011, 2012) report mass models for the elliptical galaxies NGC 720 and NGC 1521, which are comparable to M89 in stellar mass and gas temperature but still have extended gaseous atmospheres. They find the following characteristics: NGC 720 – stellar mass of $10^{11} M_\odot$, total mass of $10^{12} M_\odot$ inside 70 kpc, cumulative stellar and DM mass are equal at a radius of 6 kpc, gas temperature is 0.5 keV, declining outside 10 kpc; NGC 1521 – stellar mass of $4 \times 10^{11} M_\odot$, total mass of $2 \times 10^{12} M_\odot$ inside 100 kpc and $5 \times 10^{12} M_\odot$ inside 200 kpc, stellar mass exceeds DM mass out to 18 kpc, gas temperature about 0.5 keV, rising up to 0.8 keV outside 20 kpc.

Based on these constraints we experimented with DM halos between 1 and $10 \times 10^{12} M_\odot$ and found the main characteristics of the stripping independent of the exact choice. In this work we use a total DM mass of $3.16 \times 10^{12} M_\odot$. We chose the scale radii for the DM halos for our galaxy models with the compact and extended atmosphere case (see Table 1) such that we obtain an approximately flat circular velocity and gas temperature profile out to ~ 40 kpc, and an entropy slope comparable to the results for NGC 720 and NGC 1521. The cumulative gravitating mass and the gravitational acceleration in the central 3 kpc are almost identical between our models, and the pressure profiles agree within 25% between 1 and 8 kpc from the galaxy center.

A.2. *Galaxy orbit/ICM wind*

A.2.1. *Observational constraints*

M89 is currently located 350 kpc (72 arcmin) east of M87 in projection. The position of M89 along our LOS inside the Virgo cluster is uncertain. Tonry et al. (2001) place it at the same distance as M87, but surface brightness fluctuation measurements by Mei et al. (2007) suggest M89 is about 1 Mpc closer to us than the Virgo center. Also from surface brightness fluctuations, Blakeslee et al. (2009) list a distance of 16 ± 0.5 Mpc, which is 0.7 Mpc closer than their listed M87 distance (16.7 ± 0.6 Mpc), but consistent with the distance of M87 within the error bars.

M89 is moving towards us at $725\,{\rm km\,s^{-1}}$ or $967\,{\rm km\,s^{-1}}$ w.r.t. the Virgo mean or M87, respectively. This is close to the Virgo ICM sound speed. Its gas tail to the south and its contact discontinuity to the north suggest a signifiant velocity in the plane of the sky towards the north. Machacek et al. (2006) derive an absolute velocity of M89 through the Virgo ICM of $1700\,{\rm km\,s^{-1}}$ (Mach 2.2), based on its stagnation point pressure and assuming M89 and the Virgo center have the same distance to us. This velocity is rather high. Assuming M89 was at a larger real-space distance to the Virgo center (M87) would increase the total velocity even more, because the ambient reference pressure would be even lower, and the measured high stagnation pressure could be achieved only by a higher velocity. A velocity higher than Mach 2 at a cluster-centric distance of $\gg 300$ kpc is unlikely, hence we assume that M89's projected cluster-centric distance is close to the real-space distance. Given its projected northward motion and location straight east of the cluster center, M89 is most likely just passing the pericenter of its orbit through Virgo. This geometry is supported by our comparison between observations and simulations

Table 2
ICM parameters for the Virgo cluster model, updated version from Roediger et al. (2011).

density:	double β profile	
core radii $r_{1,2}$/ kpc:	1.7	21.4
core densities $\rho_{01,02}$/(g cm^{-3}):	$3.38 \cdot 10^{-25}$	$1.175 \cdot 10^{-26}$
$\beta_{1,2}$:	0.42	0.47
temperature:	see Eqn. 1 in Roediger et al. (2011)	
slopes $m_{1,2}$/(K pc^{-1}):	0.	0.
$T_{01,02}$/(keV):	1.53	2.4
break radius $r_{\rm break}$/ kpc:	22.6	
break range $a_{\rm break}$/ kpc:	6.7	

(paper III). If M89 was indeed 1 Mpc closer to us than the Virgo center and still moving towards us, it would have passed its pericenter many 100 Myr ago, and should have lost its remnant tail. The presence of the long remnant tail in M89 thus argues against this scenario, and instead places M89 close to pericenter passage.

With a real space velocity of 1700 km s^{-1} and a radial velocity of 725 km s^{-1} towards us, M89's orbit would be inclined by 25 degree out of the plane of the sky. Machacek et al.'s estimate of the total velocity does not include effects of ICM falling into the M89 potential from the upstream region and may thus somewhat overestimate the orbital velocity. Even if the true orbital velocity would be as low as 1000 km s^{-1}, the orbit would be inclined out of the plane of the sky by only 45 degree.

A.2.2. *ICM wind in simulation box*

For simplicity we run our simulations in the rest frame of the galaxy, i.e., the galaxy is exposed to an ICM flow or wind. This wind has a constant direction but varies in density and velocity according to the assumed motion of the galaxy through the Virgo cluster. Varying the ICM wind requires shifting the cluster potential through the simulation grid to account for the non-inertial rest frame. We neglect gradients in the ICM and cluster potential perpendicular to the orbit, i.e., we approximate the galaxy's motion through the cluster by a 'straight wind tunnel'. This is a good approximation as long as the galaxy does not pass close to the cluster center, which is the case for M89.

We calculate the variable ICM wind as follows: We set up a spherical model for the Virgo cluster. Radial ICM density and temperature profiles are described by a double beta model and Eqn. 1 in Roediger et al. (2011), respectively. Table 2 lists our updated parameters, now taking into account the measurements out to the Virgo virial radius by Urban et al. (2011). We neglect the temperature decrease beyond 400 kpc in order to keep a constant dynamic viscosity during infall in our simulations. Figure 9 summarizes available observational data and our fits. We assume the Virgo ICM is in hydrostatic equilibrium and calculate the corresponding radial gravitational acceleration and mass.

We approximate the orbit of M89 by a test particle orbit in the Virgo potential. Such test particle orbits curve only slightly at pericenter passage, hence we use the straight wind tunnel approximation as explained above. The pericenter distance is 350 kpc as observed for M89. We consider two orbits with apocenter distances of 1 and 2 Mpc and refer to them as the slow and fast orbit, respectively. The variation of ICM density, velocity, and ram pressure along these orbits is shown in Fig. 10. On these orbits, M89 reaches pericenter velocities of 1050 km s^{-1} and 1350 km s^{-1}, respectively. Both are below the estimated total velocity despite the large apocenter distances. This again suggests that the velocity from the stagnation point method is somewhat overestimated due to the upstream attraction of ICM into the M89 potential.

We want to ensure that the simulated galaxy reaches a quasi-equilibrium state and flow patterns are not dom-

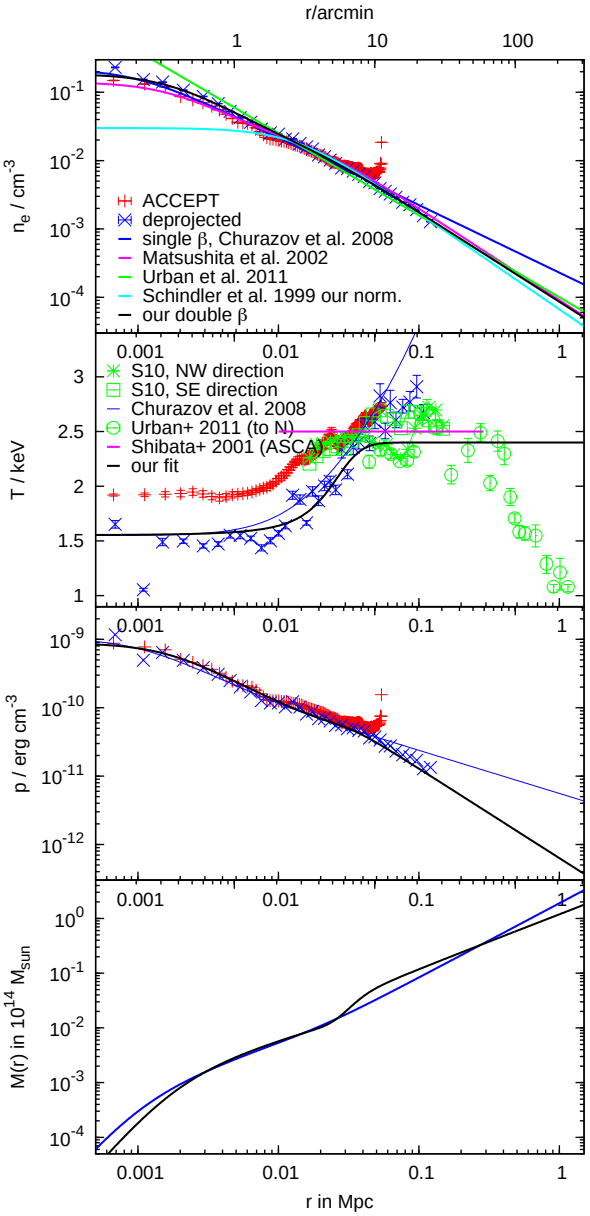

Figure 9. Virgo cluster radial profiles, from top to bottom: (i) Electron density, n_e, from the ACCEPT sample (Cavagnolo et al. 2009) and the deprojected profile (Churazov, private comm.), along with a single- or double-β model fits from Churazov et al. (2008), Matsushita et al. (2002), Urban et al. (2011), Schindler et al. (1999), and our fit. (ii) Temperature, from Simionescu et al. (2010) in two sectors, Churazov et al. (2008), Urban et al. (2011), Shibata et al. (2001), and our fit. (iii) Resulting pressure profile for selected data sets/fits, and (iv) corresponding cumulative mass profile for the Virgo cluster.

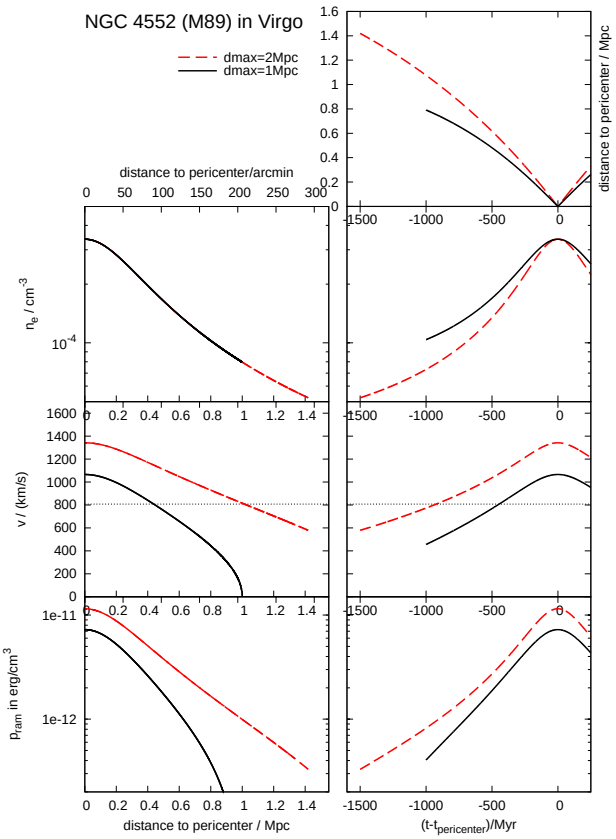

Figure 10. ICM properties along orbits, as function of position and as function of time.

inated by initial conditions. Expecting an extended relaxation phase as explained in Sect. 3, we initialize the galaxy and its motion a generously long time and distance away from the pericenter ($\geq 1\,\mathrm{Gyr}$, $\geq 0.8\,\mathrm{Mpc}$). The gentlest initialization would be to start the infall from zero velocity. With much simulation time spent in the far outskirts of the cluster it would, however, be prohibitively expensive. Therefore we start our simulations with a subsonic ICM velocity of around Mach 0.6. The initial ICM flow is set as a potential flow past the initially spherical galactic atmosphere (first panel in Fig. 1). The abrupt but subsonic onset of the flow is probably even more realistic than a fully smooth start, because in cluster outskirts subsonic large-scale turbulence or bulk flows are expected to inflict abrupt changes in the ICM wind working on the infalling galaxy.